AGU PUBLICATIONS

Geophysical Research Letters

RESEARCH LETTER
10.1002/2016GL070286

Key Points:
- Scattering due to interface topography modeled by a Monte Carlo particle method
- Fine-scale topography on the core-mantle boundary is the most likely cause of $PKKP_{bc}$ precursors
- Reduced velocity gradient in the lowermost outer core improves fits to *PKKP* precursor amplitudes at certain ranges

Correspondence to:
N. Mancinelli,
nicholas_mancinelli@brown.edu

Citation:
Mancinelli, N. and P. Shearer (2016), Scattered energy from a rough core-mantle boundary modeled by a Monte Carlo seismic particle method: Application to *PKKP* precursors, *Geophys. Res. Lett.*, *43*, doi:10.1002/2016GL070286.

Received 6 JUL 2016
Accepted 21 JUL 2016
Accepted article online 23 JUL 2016

Scattered energy from a rough core-mantle boundary modeled by a Monte Carlo seismic particle method: Application to *PKKP* precursors

Nicholas Mancinelli[1] and Peter Shearer[2]

[1]Department of Earth, Environmental and Planetary Sciences, Brown University, Providence, Rhode Island, USA, [2]Scripps Institution of Oceanography, University of California, San Diego, La Jolla, California, USA

Abstract We stack a large global data set of 1 Hz *PKKP* waveforms to constrain globally averaged properties of *PKKP* precursors. We find that the precursor observations are better explained by scattering from core-mantle boundary (CMB) topography than by scattering from the near surface, lower mantle, outer core, or inner core. However, as previously noted, simple models of CMB topography and standard 1-D seismic velocity models fail to model the range dependence of the relative amplitude between $PKKP_{bc}$ and its precursors. We find that this systematic mismatch is due, at least in part, to the assumed velocity gradient in the lowermost 250 km of the outer core. Our globally averaged *PKKP* precursor observations are consistent with random CMB topography with RMS variations of ~390 m and a horizontal correlation length of ~7 km.

1. Introduction

High-frequency scattered energy associated with *PKKP*—a core phase reflected from the underside of the core–mantle boundary—has been observed since the 1970s [*Doornbos*, 1974]. Short-wavelength topography on the core-mantle boundary (CMB) is capable of generating precursors to $PKKP_{bc}$ [*Chang and Cleary*, 1981], but simple models of CMB scattering are unable to match the range dependence displayed in the data: synthetic precursors tend to be too strong at short ranges (80–90°) and too weak at long ranges (100–110°) [*Earle and Shearer*, 1997]. Observations of the scattered energy by the Large Aperture Seismic Array (LASA) suggest that $PKKP_{bc}$ precursors may be strongly contaminated by *P•PKP*—teleseismic *P* energy that scatters to *PKP* near or at the Earth's surface [*Earle*, 2002] (Figure 1).

In this paper, we reproduce the observations of *Earle and Shearer* [1997] by stacking a global data set of ~16,000 high-quality *PKKP* waveforms recorded from 1990 to 2013. We use a Monte Carlo seismic particle approach [e.g., *Shearer and Earle*, 2004] to forward model the observations, and we confirm that simple models where energy is scattered by CMB topography generate precursors with a range dependence that systematically mismatches the observations. To address the possibility of scattered energy from other regions within the Earth, we explore a broad set of models that account for these potential contributions, including scattering from the inner core, from the lower mantle, and from the lithosphere. We find many models that excite precursory energy to $PKKP_{bc}$, but none that match the range dependence of the observations within their estimated errors.

After failing to find a scattering geometry that explains the range dependence seen in the data, we explore the possibility that changes to the underlying 1-D velocity model could modulate the amplitudes of $PKKP_{bc}$ precursors. Observed PKP_{bc} traveltime residuals from *Souriau* [2015] imply that standard 1-D velocity models such as *ak*135 need a decreased velocity gradient about 250 km above the inner-core boundary (ICB). We design 1-D velocity models that fit absolute PKP_{bc} traveltimes from *Souriau* [2015] and find that these models change the range dependence of our synthetics to be more like that which is observed. This result supports CMB scattering as the primary cause of $PKKP_{bc}$ precursor energy and suggests that large-scale lateral variations in outer-core velocity structure modulate the relative amplitudes of $PKKP_{bc}$ precursors.

2. Methods

2.1. Data Stacking

We begin our analysis with a collection of 604,626 broadband vertical (i.e., BHZ) seismograms from 7696 events occurring from 1990 to 2013, recorded at epicentral distances between 70° and 120°.

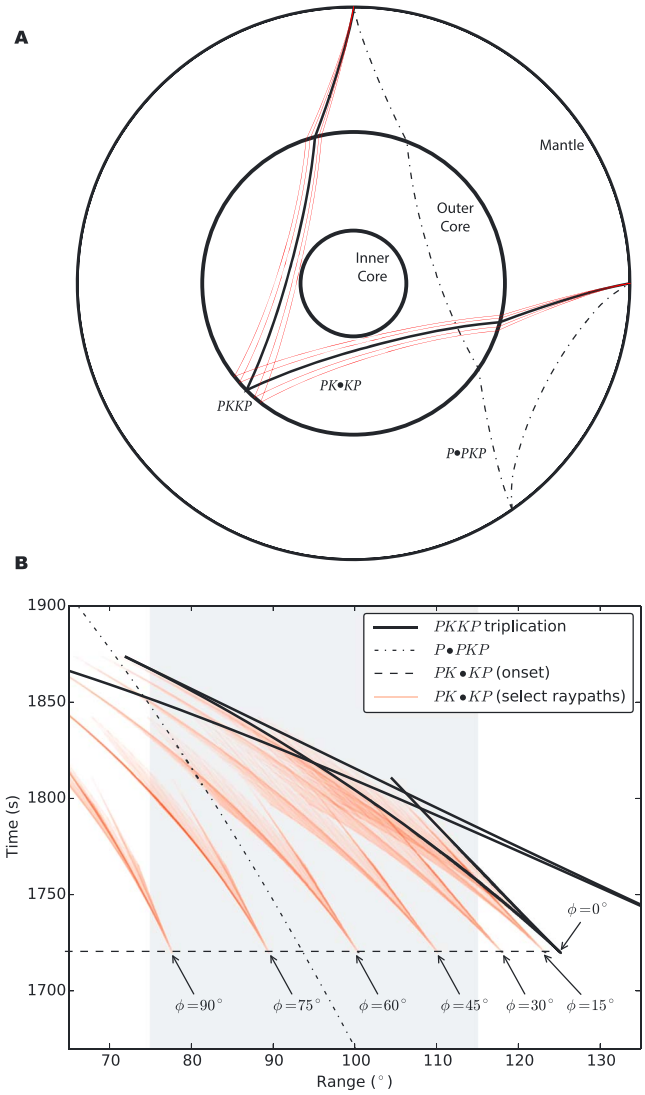

Figure 1. (a) Raypaths for *PKKP*, *PK•KP*, and *P•PKP* traveling within the diametrical plane. (b) Traveltime curves for *PKKP*, *PK•KP*, and *P•PKP*. *PKKP* is the underside reflection from the CMB and is predicted by 1-D Earth models. *PK•KP* scatters at the CMB underside reflection point. This energy may be scattered out of plane; ϕ represents the change in ray azimuth at the scattering point [cf., *Rost et al.*, 2015]. *P•PKP* scatters from teleseismic *P* into the *PKP b*-caustic—or vice versa—near the Earth's free surface. The range of epicentral distances considered in this study is shaded in gray.

The seismograms are windowed around $PKKP_{bc}$ and, after applying an antialiasing filter, downsampled to 10 Hz. We apply a stacking procedure similar to *Earle and Shearer* [1997], following the strategy outlined by *Shearer and Earle* [2008]. In brief, each seismogram is filtered between 0.7 and 2.5 Hz and aligned on the ray-theoretical arrival time of $PKKP_{bc}$. We reject waveforms that exhibit signal-to-noise amplitude ratios lower than $\sqrt{1.9}$—a value chosen to minimize the variance of the stack as estimated by bootstrap resampling. Changes in the placement and width of the noise window affect the zero offset of the final stack; we settle on a window from −140 to −80 s to be consistent with the processing method of *Earle and Shearer* [1997]. The envelope function of each high-quality seismogram is computed and converted to power. The average preevent noise power is subtracted from the entire trace, and the resulting time series is summed in an appropriate range bin.

The final stack contains a total of 16,205 seismograms; note that many have been rejected due to signal-generated noise. Figure 2 shows the spatial coverage of these data. Although much of the Earth's surface area is represented, the coverage is far from uniform. To get a sense of how close our stack is to the true global average, we apply bootstrap resampling to regional subsets of the data. We divide the Earth's surface

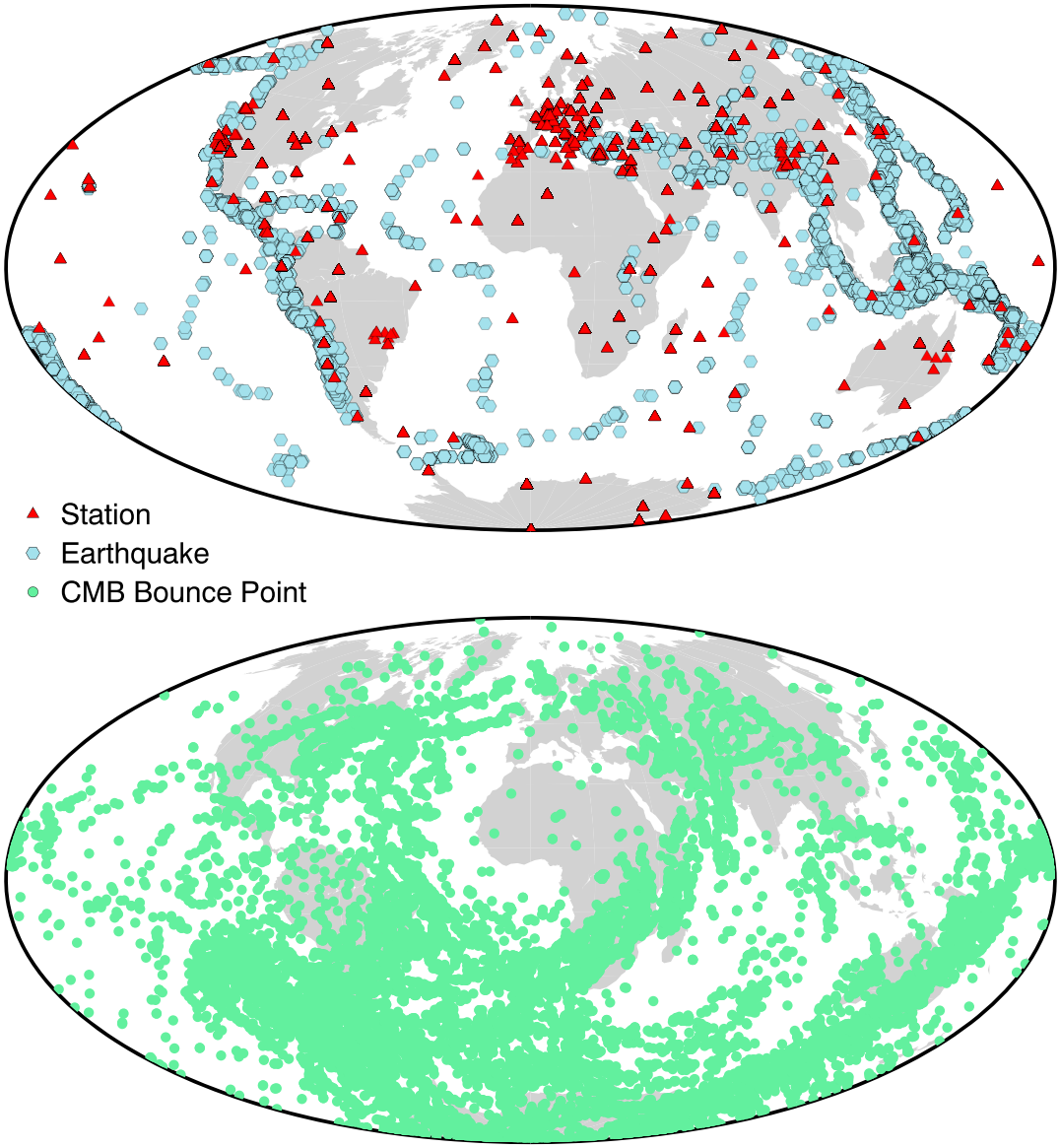

Figure 2. Spatial distribution of the *PKKP* data set used in this study. (top) The source-receiver locations for the ~17,000 recordings that passed our signal-to-noise test; (bottom) corresponding CMB underside reflection points.

into 104 cells, each about 20° across. Each seismogram is assigned two integers, i and j, that index the source and receiver cells, respectively. Of course, not all (i, j) combinations are populated because the ray geometry of this phase is limited to a small range of epicentral distances and the source and receiver distributions are nonuniform. The number of populated substacks is between 124 and 274 depending on the particular range bin. The seismograms are grouped with others of the same (i, j) pair. For each bootstrap sample, data are combined from a random selection of the populated groups and stacked. The mean of the 1000 bootstrap samples provides our estimate for the global average; the square root of the variance provides an estimate of the standard error. These are plotted for each range bin in Figure 3.

2.2. Waveform Modeling

To model the global stack, we use a particle-based Monte Carlo phonon algorithm. This method has been used in previous studies to model energy scattered from volumetric heterogeneity [*Shearer and Earle*, 2004; *Peng et al.*, 2008; *Mancinelli and Shearer*, 2013; *Mancinelli et al.*, 2016a, 2016b], but it has not yet been used to model scattering from interface topography. *Bataille and Flatté* [1988] and *Bataille et al.* [1990] derived a theory based on the Kirchhoff-Helmholtz method where the average scattered power at a given point is

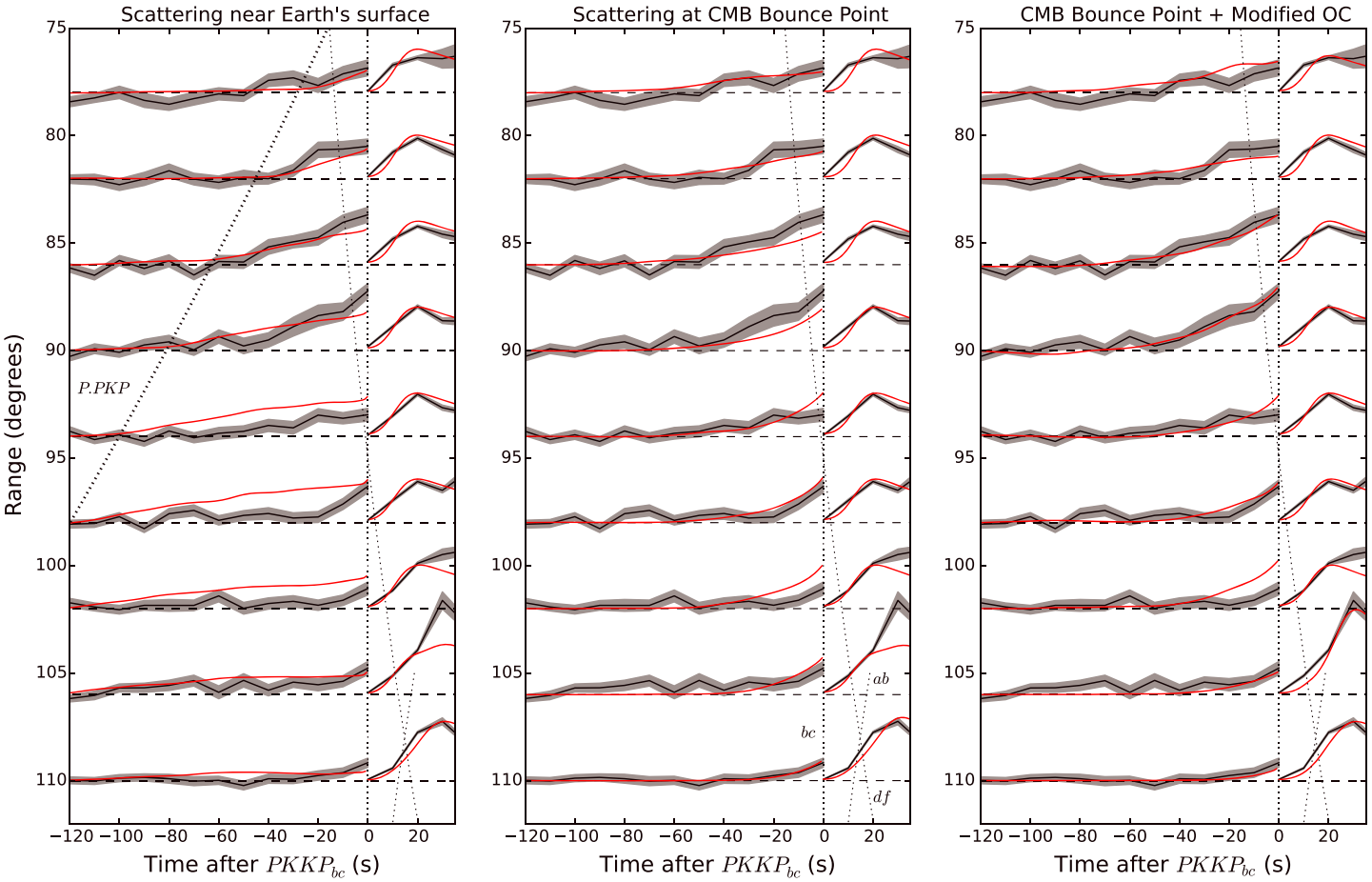

Figure 3. Globally averaged *PKKP* precursor stacks (black); the standard error of the mean is shown by gray shading. The red curves represent phonon code predictions for scattering (left) in the uppermost 200 km of the mantle, (middle) at the CMB reflection point, and (right) at the CMB reflection point with a decreased gradient in the outer core. The precursors are scaled by a factor of 15 to enhance visibility. The thick dotted line in Figure 3 (left) delineates onset times for *P•PKP* scattering at the Earth's surface. At each range, the synthetics are multiplied by a scaling factor, shifted by up to 3 s to account for uncertainties in the velocity model, and convolved with an empirical function to model the coda decay.

computed by summing scattering contributions from the entire CMB interface. Their theory suggests that (1) the scattered power scales linearly with the mean square fluctuation of the topographic surface (provided that the perturbations are < 1 km) and (2) the scattering pattern is directly related to the two-dimensional (2-D) Fourier transform, $\Phi(\mathbf{k})$, of the topography autocorrelation function where the wave number vector $\mathbf{k} = \omega/\alpha\left(\hat{\mathbf{r}} - \hat{\mathbf{s}}\right)$ and $\hat{\mathbf{r}}$ and $\hat{\mathbf{s}}$ are unit vectors describing the directions of the specular reflection and the scattered wave, respectively. More concretely, the intensity radiated by the rough surface is given by

$$I(\mathbf{k}) = A^2R^2||\mathbf{k}||^2\left[\delta(\mathbf{k}) + ||\mathbf{k}||^2\Omega\,\Phi\,(\mathbf{k})\right], \tag{1}$$

where A is the amplitude of the incident wave, R is the reflection coefficient, and Ω depends upon geometry and the elastic parameters of the media on either side of the interface [*Bataille and Flatté*, 1988, equation (A19)]. In this study, we assume that the elastic parameters do not change with topography, so $\Omega = (\alpha T')^2$, where α is the P velocity just beneath the CMB and T' is the change in traveltime with respect to change in topography. For rays near the b-caustic, Ω is about 1.3. The total probability that a reflected phonon scatters away from the specular direction is given by integrating the second term over all directions, i.e.,

$$P_s = ||\mathbf{k}||^2 \iint \Omega\Phi\left[||\mathbf{k}||\left(\hat{\mathbf{r}} - \hat{\mathbf{s}}\right)\right] \mathrm{d}\hat{\mathbf{s}}. \tag{2}$$

To simulate the effects of CMB topography on *PKKP*, we directly define a scattering probability, P_s, and a distribution of scattering angles (e.g., zero-mean Gaussian with width, σ). After finding a working model,

we can estimate the correlation length, a, of Gaussian topography from the 2-D Fourier transform, i.e.,

$$a = \frac{\alpha}{\sqrt{2}\omega \sin\frac{\sigma}{2}} \tag{3}$$

and the RMS fluctuation in topography, ζ, by applying numerical integration to equation (2) assuming

$$\Phi(\mathbf{k}) = \frac{\zeta^2}{4\pi} a^2 e^{-||\mathbf{k}||^2 a^2/4} \tag{4}$$

$$\Omega = 1.3\,. \tag{5}$$

The advantage of this theory is that it directly relates the statistical properties of a rough surface to scattering probabilities. This is in contrast to the approach taken by *Earle and Shearer* [1997], who generated Kirchhoff synthetics from specific realizations of random topography.

3. Scattering Throughout the Earth

Fine-scale seismic structure is likely present in nearly every depth range throughout the Earth, perhaps excepting the liquid outer core (see *Shearer* [2015] for a recent review). In this section, we explore the possibility of scattering contributions to the observed *PKKP* precursors from many of these depth ranges including the core, the lower mantle, and the shallow Earth.

3.1. Inner-Core Scattering and *PKIJKP*

Strong scattering by small-scale structure within the solid inner core has been proposed previously by several studies. *Vidale and Earle* [2000] and *Peng et al.* [2008] modeled *PKiKP* coda as backscattered energy originating from just beneath the inner-core boundary. It has also been suggested that strong, small-scale heterogeneity throughout the inner core could be primarily responsible for inner-core attenuation observed at frequencies near 1 Hz [*Cormier et al.*, 1998].

We find, however, that heterogeneity within the inner core does not produce observable precursors to $PKKP_{bc}$, provided that one assumes a realistic value for the inner-core attenuation, $1/Q_\alpha$. If one relaxes this constraint and allows for arbitrarily large inner-core Q_α, *PKIJKP*—a core phase with an underside reflection and conversion at the inner-core boundary—becomes visible in the precursor window of the synthetics. This phase displays large amplitudes at short ranges and small amplitudes at long ranges, as do the observations, but the emergent nature of the observed precursors is not well matched by this candidate, as *PKIJKP* is not a scattered phase. Moreover, it is unlikely that *PKIJKP* can be seen in global stacks, given what is known about the attenuation structure of the inner core [c.f., *Bhattacharyya et al.*, 1993].

Topography on the inner-core boundary [e.g., *Cao et al.*, 2007] may also scatter energy; we did not explicitly test this scenario because the ray geometries involved are expected to be very similar to those of energy scattered by inner-core heterogeneity.

3.2. Outer-Core Scattering

Although it is generally assumed that the fluid outer core is well mixed [*Stevenson*, 1987], we test to see if scattering in this region might contribute energy to the observed signal. Backscattering from a heterogeneous layer at the top of the outer core with variable thickness between 100 and 300 km indeed generates precursors to $PKKP_{bc}$ in our synthetics. These behave much like those produced from CMB topography: they are too large at ranges $> 90°$ and too small at ranges $< 90°$. Forward scattering in the outer core is unlikely based on evidence from *PKP* precursor onset times, but backward scattering is permissible. However, it is difficult to imagine a mechanism that scatters energy in the backward direction only, so we pursue this candidate no further.

3.3. CMB Topography

Of all the scattering models that we tried, CMB topography produces synthetics that most closely resemble the observed data stacks. The observations are best matched when 20% of the CMB-reflected energy is scattered according to Gaussian scattering probabilities with a width of 15° (Figure 3, middle). Increasing the overall scattering probability tends to increase the scattered amplitudes at all times. Increasing the Gaussian width (i.e., increasing the average scattering angle) tends to affect the time dependence of the precursor energy; larger angles generally redirect a greater proportion of energy to earlier times. The main problem with

these models, again, is that they systematically underpredict the observations at short ranges and overpredict the observations at long ranges. We find that our preferred model is associated with a Gaussian correlation length of 7 km and an RMS topography fluctuation of 390 m, which is slightly outside the range of 250–350 m reported by *Earle and Shearer* [1997].

3.4. Lower Mantle Scattering

Volumetric heterogeneity in the lower mantle also excites visible precursors to $PKKP_{bc}$, provided that the RMS perturbations are on the order of 1%. This model is problematic for two reasons: (1) synthetics associated with this model display a wide bump of strong energy from −60 to −20 s at ranges near ∼86°, whereas the observations show no such feature and (2) it is difficult to reconcile this model with observations of *PKP* precursors that suggest weak small-scale variations on the order of 0.1% in the lowermost mantle [*Margerin and Nolet*, 2003; *Mancinelli and Shearer*, 2013].

3.5. Scattering Near the Earth's Surface

Finally, structure near the Earth's surface can produce precursors to $PKKP_{bc}$. This energy is thought to be scattered from teleseismic *P* to *PKP*, or vice versa, near or at the underside reflection from the free surface. The focusing effect of the *b* caustic amplifies this energy, termed *P•PKP*, and is likely responsible for $PKKP_x$ — high-frequency energy observed at ranges beyond the *c* caustic [*Earle and Shearer*, 1998; *Earle*, 2002].

Synthetic tests show that both volumetric heterogeneity in the lithosphere/upper mantle and topography at the Earth's surface can generate precursors to $PKKP_{bc}$. This model is problematic, however, because these precursors have much earlier onset times than those observed (Figure 3, left), particularly at long ranges. Moreover, synthetics associated with this model display relatively constant power at greater times; this is at odds with the emergent nature of the observed energy.

It is interesting that the heterogeneity parameters for the lithosphere and upper mantle published by *Shearer and Earle* [2004] predict synthetic precursors that are much larger than the observations (not shown). This suggests that either (1) the strength of *P• PKP* varies laterally and our signal-to-noise check is doing its job of rejecting the set of seismograms that are contaminated by this energy or (2) the *Shearer and Earle* [2004] model underestimates the role of intrinsic attenuation in the mantle, and thus, *P•PKP* retains too much energy. Explanation (1) is more likely due to the clear observations of *P•PKP* made at LASA by *Earle* [2002].

It may be that both *P•PKP* and CMB topography contribute energy to the global stacks, but we did not find that linear combinations of energy scattered by these two mechanisms led to appreciably better results than those given by the simple model of CMB topography alone. Thus, we argue that scattering from CMB topography is the most plausible mechanism for the observed precursors to $PKKP_{bc}$. In the following section, we show that improved fits can be achieved in certain range bins through more careful modeling of the reference phase $PKKP_{bc}$.

4. The Validity of Ray Theory

One possible reason that scattering models might fail to match the observed range dependence is if ray theory breaks down for rays turning near the ICB. This would result in lower relative $PKKP_{bc}$ amplitudes at short ranges near the *c* caustic, as finite-frequency waves begin to sense inner-core structure. We test this idea by generating ∼1 Hz reflectivity synthetics [e.g., *Choy et al.*, 1980] for the *bc* branch. This involves applying the Earth flattening transformation to *iasp*91 and approximating the result with a model of 500 uniform layers. The layer thicknesses vary with depth but are around 20–30 km (in flat Earth coordinates) within the vicinity of the ICB. We generate synthetic seismograms accurate to 1.05 Hz for slowness values between 0.005 and 0.07 s/km; the slowness spacing is on the order of 10^{-6} s/km. The result of this test, shown in Figure 4, indicates that the amplitudes of $PKKP_{bc}$ are only significantly affected by finite-frequency effects at ranges less than ∼78°. Since we are concerned with improving the fits at ranges between 80° and 100°, it is unlikely that the limitations of ray theory are causing the systematic misfits to the observations.

5. Sensitivity to the Outer-Core Velocity Gradient

Another factor that affects the amplitude of $PKKP_{bc}$ is geometrical spreading. This is handled in the phonon code by counting the number of phonons that return to the free surface in any given time range bin. Increasing (or decreasing) the velocity gradient in a particular depth range refracts more (or fewer, respectively) phonons

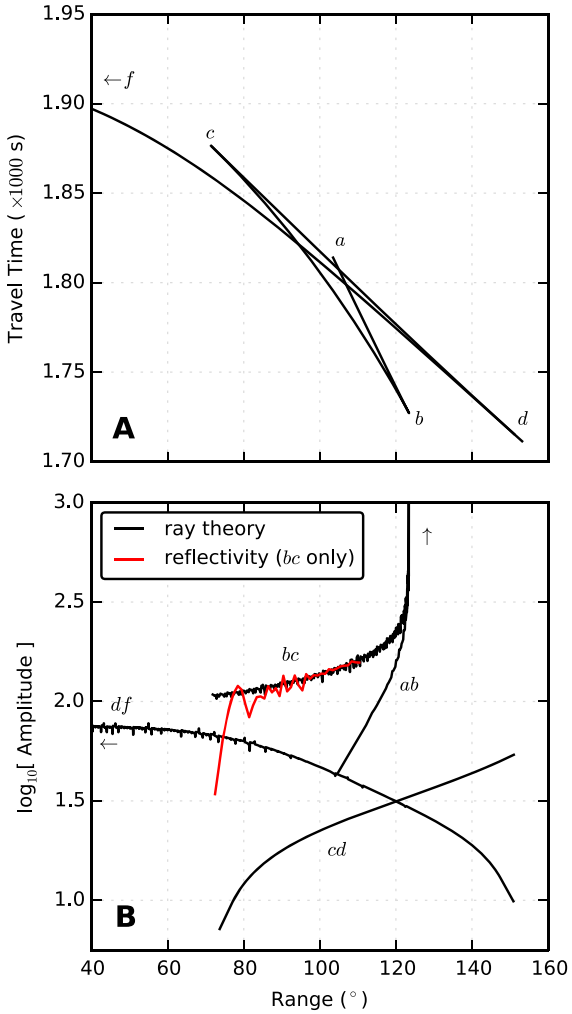

Figure 4. (a) Ray-theoretical traveltimes of the *PKKP* triplication for velocity model *iasp*91. (b) Comparison between ray-theoretical and 1 Hz reflectivity amplitudes for $PKKP_{bc}$. On the *bc* branch near the *c* caustic, the reflectivity amplitudes decrease more rapidly than the ray-theoretical amplitudes as finite-frequency waves begin to sense inner-core structure. Note that all amplitudes are relative and that the $PKKP_{df}$ amplitudes shown do not include the effects of inner-core attenuation or the transmission coefficient at the ICB.

into a particular range bin at the free surface. Thus, the amplitude of the $PKKP_{bc}$ branch can be reduced near the *c* caustic by reducing the *P* velocity gradient just above the ICB. Likewise, the amplitude of the $PKKP_{bc}$ branch can be increased away from the *c* caustic by increasing the *P* velocity gradient in a layer located a few hundred kilometers above the ICB.

In this section, we attempt to find a model that improves fits to the $PKKP_{bc}$ precursor amplitudes while maintaining reasonable fits to PKP_{bc} traveltimes. As a first step, we replace our initial 1-D model, *iasp*91 [*Kennett and Engdahl*, 1991], with its update, *ak*135 [*Kennett et al.*, 1995], which is highly similar to *iasp*91, except in the region above the ICB where a reduced velocity gradient is imposed to provide better fits to the core phases. Upon first glance, model *ak*135 is appealing because it features a layer of reduced velocity gradient above the ICB. After generating synthetics from this model, however, we find no significant difference to the data fits.

While *ak*135 is generally accepted as one of the best models for modeling the traveltimes of a broad range of core phases, it does not perfectly match the observed traveltimes of every individual phase. Observed traveltime residuals of PKP_{bc} with respect to *ak*135 suggest a decreased gradient at depths in a layer 0–300 km above the ICB [*Souriau*, 2015, Figure 2b]. We design several 1-D velocity models that satisfy the general

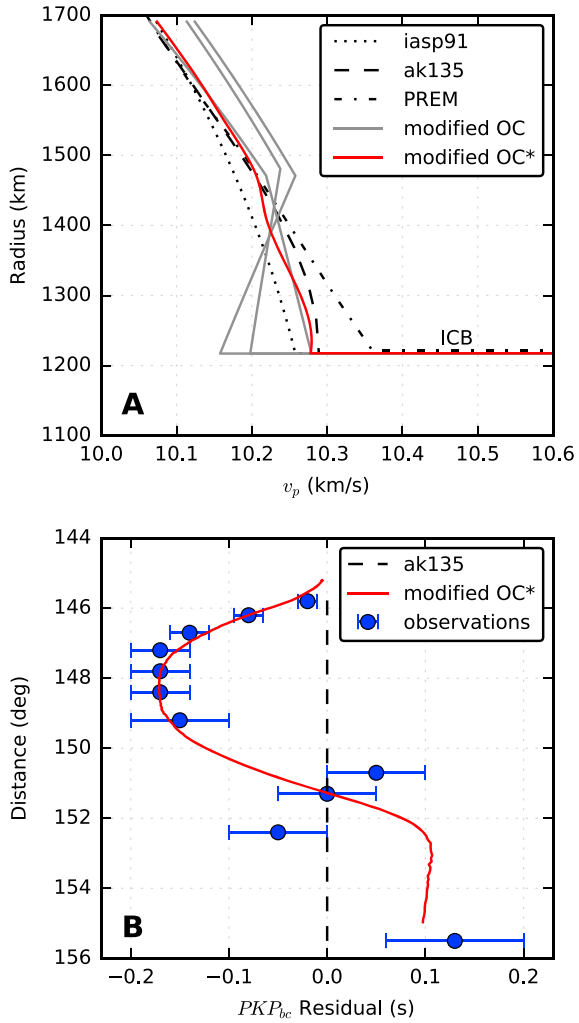

Figure 5. (a) One-dimensional reference models of the lowermost outer core. The initial model we use is *iasp*91 [*Kennett and Engdahl*, 1991]; models *ak*135 [*Kennett et al.*, 1995], and PREM [*Dziewonski and Anderson*, 1981] are plotted for comparison. The collection of models plotted in gray change the range dependence of the *PKKP* precursors. The model plotted in red changes the range dependence of the synthetics, improving fits at certain ranges, and it also predicts ray-theoretical traveltimes that match the general character of the PKP_{bc} residuals measured by *Souriau* [2015]. (b) Comparison between the observed traveltime residuals (blue) reported by *Souriau* [2015] (blue) and the ray-theoretical prediction corresponding to the model denoted by an asterisk (red).

character of traveltime constraints; most share the common feature of a reduced velocity gradient at about 250 km above the ICB. We find that these reduced velocity gradients affect the range dependence of the $PKKP_{bc}$ precursor amplitudes, yet we cannot find a single model that fits all of the details imaged by the global stack.

In this paper we show one such model that improves the fits at 86° and 90° by increasing the relative precursor amplitudes at these ranges (Figure 3, right). An additional (and unexpected) improvement occurs at 106°, where the direct $PKKP_{ab}$ amplitude resembles the data more closely than before. The most apparent flaw of this model appears at 102°, where the synthetic precursor amplitudes are much larger than those observed. This may be due to the tunneling effect of the *ab* branch past the *a* point, which would likely increase the amplitude of the reference phase at 102°. Future modeling should attempt to account for the effect of this tunneling, as it is thought to be a key process for energy that reflects beneath the CMB, even at 1 Hz [*Richards*, 1973]. The model we show in Figure 5 does not include the secondary kink required to fit all of Souriau's observations. In testing such a model, we found the synthetic amplitudes to vary rapidly from range bin to range bin, whereas the observed transition is more gradual.

Although we do not find a single model that satisfies all of the details shown in the data stack, this result shows that changing the velocity gradient at the base of the outer core modulates the range dependence of the synthetic precursors. Thus, our inability to find a single model that matches the stack at all ranges may point toward lateral variations in outer-core structure. Unfortunately, we are unable to resolve this issue given the data quality: stacking regional subsets of the data results in larger error bars which preclude observations of lateral variations in precursor strength.

6. Discussion

Several previous studies support the idea of a decreased velocity gradient in the lowermost outer core, suggesting a change in composition (or phase) that raises the density of the fluid approaching the ICB. To model PKP_{bc} and PKP_{c}-diffracted traveltimes, *Souriau and Poupinet* [1991] used a liquid core model in which the velocity is constant in the lowermost 150 km of the fluid core. *Song and Helmberger* [1992] modeled *PKP* waveforms with a low-velocity gradient in the lowermost 400 km of the fluid core. This resulted in the proposal of preliminary reference Earth model version (PREM2) [*Song and Helmberger*, 1995], a *P*-velocity model for the core that shows a better fit to *PKP* differential traveltimes, amplitude ratios, and waveforms than does PREM [*Dziewonski and Anderson*, 1981]. PREM2 is much like *ak*135, having nearly constant velocity throughout the lowermost 100 km of the outer core.

More recently, *Yu et al.* [2005] argue for large-scale lateral variability in lowermost outer-core structure using differential traveltimes, waveforms, and amplitude ratios of core phases. Rays traversing the Eastern Hemisphere are best explained by PREM, whereas data traversing the Western Hemisphere are better explained by another model (called OW) that has reduced velocities relative to PREM in the lowermost 200 km of the outer core. Another study by *Zou et al.* [2008] found that traveltimes of *PKPc*-diffracted favor models with a reduced gradient like *ak*135, while *PKPc*-diffracted amplitudes favor PREM-like models. The authors suggest that this paradox may be reconciled by introducing low Q_{α} throughout the bottom 350 km of the outer core. *Adam and Romanowicz* [2015] report global observations of a mystery (M-) phase, which likely represents scattered energy from the vicinity of the inner-core boundary. *Adam and Romanowicz* [2015] tentatively explain the traveltimes of this phase by invoking an increased gradient from 100 to 400 km above the ICB with a 50 km thick low-velocity layer right above the ICB. The two regions are connected by a 50 km thick transition with a steep negative velocity gradient. We test an outer-core velocity model with a low-velocity layer similar to that proposed by *Adam and Romanowicz* [2015], but we found that this model generates precursors that are much too large at ranges from 75 to 85°, likely because the low-velocity layer dramatically reduces the direct $PKKP_{bc}$ amplitudes at ranges less than ~85°.

7. Conclusion

In summary, we test a broad range of scattering mechanisms to model $PKKP_{bc}$ precursors, ruling out significant contributions from heterogeneity within the inner core, the outer core, and the lower mantle. Scattering from teleseismic *P* to *PKP* generates strong precursors, but their time and range dependence are at odds with the observations. Thus, scattering by CMB topography remains the most likely mechanism. We show that reducing the velocity gradient 250 km above the outer core satisfies PKP_{bc} traveltime constraints adapted from *Souriau* [2015]; such changes modulate the amplitude of scattered energy at ranges between 84° and 92° and improve the fit to the observations at some ranges.

Acknowledgments

This research was supported by National Science Foundation grant EAR-1111111 and the National Science Foundation Graduate Research Fellowship Program. The facilities of IRIS Data Services, and specifically the IRIS Data Management Center, were used for access to waveforms and related metadata used in this study. IRIS Data Services are funded through the Seismological Facilities for the Advancement of Geoscience and EarthScope (SAGE) Proposal of the National Science Foundation under Cooperative Agreement EAR-1261681. The data set for this paper is available by contacting the corresponding author at nicholas_mancinelli@brown.edu. The authors are grateful for two anonymous reviews which improved the quality of this manuscript.

References

Adam, J.-C., and B. Romanowicz (2015), Global scale observations of scattered energy near the inner-core boundary: Seismic constraints on the base of the outer-core, *Phys. Earth Planet. Inter.*, *245*, 103–116, doi:10.1016/j.pepi.2015.06.005.

Bataille, K., and S. M. Flatté (1988), Inhomogeneities near the core-mantle boundary inferred from scattered PKP waves recorded at the Global Digital Seismograph Network, *J. Geophys. Res.*, *93*(B12), 15,057–15,064, doi:10.1029/JB093iB12p15057.

Bataille, K., R. S. Wu, and S. M. Flatté (1990), Inhomogeneities near the core-mantle boundary evidenced from scattered waves: A review, *Pure Appl. Geophys.*, *132*(1–2), 151–173, doi:10.1007/BF00874361.

Bhattacharyya, J., P. Shearer, and G. Masters (1993), Inner core attenuation from short-period *PKP*(*BC*) versus *PKP*(*DF*) waveforms, *Geophys. J. Int.*, *114*(1), 1–11, doi:10.1111/j.1365-246X.1993.tb01461.x.

Cao, A., Y. Masson, and B. Romanowicz (2007), Short wavelength topography on the inner-core boundary, *Proc. Natl. Acad. Sci.*, *104*(1), 31–35, doi:10.1073/pnas.0609810104.

Chang, A. C., and J. R. Cleary (1981), Scattered *PKKP*: Further evidence for scattering at a rough core-mantle boundary, *Phys. Earth Planet. Inter.*, *24*(1), 15–29, doi:10.1016/0031-9201(81)90075-3.

Choy, G. L., V. F. Cormier, and R. Kind (1980), A comparison of synthetic seismograms of core phases generated by the full wave theory and by the reflectivity method, *J. R. Astron. Soc.*, *61*(1), 21–39, doi:10.1111/j.1365-246X.1980.tb04301.x.

Cormier, V. F., L. Xu, and G. L. Choy (1998), Seismic attenuation of the inner core: Viscoelastic or stratigraphic?, *Geophys. Res. Lett.*, *25*(21), 4019–4022.

Doornbos, D. J. (1974), Seismic wave scattering near caustics: Observations of *PKKP* precursors, *Nature*, *247*(5440), 352–353, doi:10.1038/247352a0.

Dziewonski, A. M., and D. L. Anderson (1981), Preliminary reference Earth model, *Phys. Earth Planet. Inter.*, *25*(4), 297–356.

Earle, P. S. (2002), Origins of high-frequency scattered waves near PKKP from Large Aperture Seismic Array data, *Bull. Seismol. Soc. Am.*, *92*(2), 751–760, doi:10.1785/0120010169.

Earle, P. S., and P. M. Shearer (1997), Observations of PKKP precursors used to estimate small-scale topography on the core-mantle boundary, *Science*, *277*(5326), 667–670, doi:10.1126/science.277.5326.667.

Earle, P. S., and P. M. Shearer (1998), Observations of high-frequency scattered energy associated with the core phase PKKP, *Geophys. Res. Lett.*, *25*(3), 405–408.

Kennett, B. L. N., and E. R. Engdahl (1991), Traveltimes for global earthquake location and phase identification, *Geophys. J. Int.*, *105*(2), 429–465, doi:10.1111/j.1365-246X.1991.tb06724.x.

Kennett, B. L. N., E. R. Engdahl, and R. Buland (1995), Constraints on seismic velocities in the Earth from traveltimes, *Geophys. J. Int.*, *122*(1), 108–124, doi:10.1111/j.1365-246X.1995.tb03540.x.

Mancinelli, N., P. Shearer, and C. Thomas (2016a), On the frequency dependence and spatial coherence of PKP precursor amplitudes, *J. Geophys. Res. Solid Earth*, *121*, 1873–1889, doi:10.1002/2015JB012768.

Mancinelli, N., P. Shearer, and Q. Liu (2016b), Constraints on the heterogeneity spectrum of Earth's upper mantle, *J. Geophys. Res. Solid Earth*, *121*, 3703–3721, doi:10.1002/2015JB012641.

Mancinelli, N. J., and P. M. Shearer (2013), Reconciling discrepancies among estimates of small-scale mantle heterogeneity from PKP precursors, *Geophys. J. Int.*, *195*(3), 1721–1729, doi:10.1093/gji/ggt319.

Margerin, L., and G. Nolet (2003), Multiple scattering of high-frequency seismic waves in the deep Earth: PKP precursor analysis and inversion for mantle granularity, *J. Geophys. Res.*, *108*(B11), 2514, doi:10.1029/2003JB002455.

Peng, Z., K. D. Koper, J. E. Vidale, F. Leyton, and P. Shearer (2008), Inner-core fine-scale structure from scattered waves recorded by LASA, *J. Geophys. Res.*, *113*, B09312, doi:10.1029/2007JB005412.

Richards, P. G. (1973), Calculation of body waves, for caustics and tunnelling in core phases, *Geophys. J. R. Astron. Soc.*, doi:10.1111/j.1365-246X.1973.tb02426.x.

Rost, S., P. S. Earle, P. M. Shearer, D. A. Frost, and N. D. Selby (2015), Seismic detections of small-scale heterogeneities in the deep Earth, in *Earth's Heterogeneous Mantle: A Geophyiscal, Geodynamical, and Geochemical Perspective*, chap. 12, pp. 367–390, Springer, New York, doi:10.1007/978-3-319-15627-9.

Shearer, P. M. (2015), Seismic scattering in the deep Earth, in *Treatise on Geophysics, Second Edition. Volume 1: Deep Earth Seismology*, edited by G. Schubert, pp. 759–787, Elsevier, Oxford, U. K., doi:10.1016/B978-0-444-53802-4.00018-X.

Shearer, P. M., and P. S. Earle (2004), The global short-period wavefield modelled with a Monte Carlo seismic phonon method, *Geophys. J. Int.*, *158*(3), 1103–1117, doi:10.1111/j.1365-246X.2004.02378.x.

Shearer, P. M., and P. S. Earle (2008), Observing and modeling elastic scattering in the deep Earth, *Adv. Geophys.*, *50*, 167–193.

Song, X., and D. V. Helmberger (1992), Velocity structure near the inner core boundary from waveform modeling, *J. Geophys. Res.*, *97*(B5), 6573–6586.

Song, X., and D. V. Helmberger (1995), A P wave velocity model of Earth's core, *J. Geophys. Res.*, *100*(B6), 9817, doi:10.1029/94JB03135.

Souriau, A. (2015), Presumption of large-scale heterogeneity at the top of the outer core basal layer, *Earth Planet. Sci. Lett.*, *415*, 175–182, doi:10.1016/j.epsl.2015.01.024.

Souriau, A., and G. Poupinet (1991), The velocity profile at the base of the liquid core from *PKP*(*BC* + *Cdiff*) data: An argument in favour of radial inhomogeneity, *Geophys. Res. Lett.*, *18*(11), 2023–2026, doi:10.1029/91GL02417.

Stevenson, D. (1987), Limits on lateral density and velocity variations in the Earth's outer core, *Geophys. J. Int.*, *88*(1), 311–319, doi:10.1111/j.1365-246X.1987.tb01383.x.

Vidale, J., and P. Earle (2000), Fine-scale heterogeneity in the Earth's inner core, *Nature*, *404*(6775), 273–275, doi:10.1038/35005059.

Yu, W.-c., L. Wen, and F. Niu (2005), Seismic velocity structure in the Earth's outer core, *J. Geophys. Res.*, *110*, B02302, doi:10.1029/2003JB002928.

Zou, Z., K. D. Koper, and V. F. Cormier (2008), The structure of the base of the outer core inferred from seismic waves diffracted around the inner core, *J. Geophys. Res.*, *113*, B05314, doi:10.1029/2007JB005316.